Monthly Notices
of the
ROYAL ASTRONOMICAL SOCIETY

MNRAS (2017)
Advance Access publication 2016 November 23

doi:10.1093/mnras/stw3027

The hierarchical triple system DY Lyncis

W. Dimitrov,[1⋆] H. Lehmann,[2⋆] K. Kamiński,[1⋆] M. K. Kamińska,[1] M. Zgórz[1] and M. Gibowski[1]

[1]*Astronomical Observatory Institute, Faculty of Physics, A. Mickiewicz University, Słoneczna 36, PL-60-286 Poznań, Poland*
[2]*Thüringer Landessternwarte Tautenburg, Sternwarte 5, D-07778 Tautenburg, Germany*

Accepted 2016 November 21. Received 2016 November 21; in original form 2016 June 7

ABSTRACT

We present the results of a six-year spectroscopic monitoring of DY Lyncis. Three different echelle spectrographs were used to collect the spectroscopic data. Each DY Lyncis spectrum contains lines of three different stars. Two of them belong to a very close eclipsing binary (EB) with an orbital period of 1.3 d. The reflex motion due to the third body can be observed in the radial velocities of the EB. We found the period of the wide orbit to be 281 d and its eccentricity is 0.33. We used the Wilson–Devinney method to fit both orbits. The analysis revealed that the EB consists of two very similar stars of 1.21 and 1.14 $M_{\odot}$, corresponding to a mass ratio of 0.94. The fit of the long-period orbit showed that the third body is the most massive component in the system, its mass is 1.40 $M_{\odot}$. Additionally, the atmospheric parameters were calculated for all three components. For that, we acquired spectra with a 2-m class telescope where we obtained sufficient signal-to-noise ratio. We derived temperatures of 6370 ± 150 and 6260 ± 140 K for the EB components, and 6380 ± 110 K for the most massive star. From the combined photometric and spectroscopic analysis, we estimate that the distance and age of the system are 285 pc and 2.5 Gyr, respectively.

Key words: binaries: close – binaries: eclipsing – binaries: spectroscopic.

1 INTRODUCTION

Stars form in multiple systems, as we know from both observations and theoretical considerations. The nearest star formation region is the Taurus molecular cloud. According to Leinert et al. (1993) and Kohler & Leinert (1998), 100 per cent of Taurus pre-main-sequence stars are binaries or multiple systems. During the dynamical evolution lighter components can be ejected from these systems.

Some of the multiples contain close pairs. According to Zasche et al. (2009), we know more than 100 multiple stars with eclipsing components. Recent spectroscopic and photometric measurements allow the absolute parameters of the eclipsing binary (EB) components to be obtained with an accuracy of 1 per cent or better. One of the main formation theories for close triple systems assumes shrinking of the inner orbit by Kozai cycles with tidal friction (Eggleton & Kiseleva-Eggleton 2001).

In 2009, we started our project of monitoring multiple stars with eclipsing components. The targets for our project are HD 86222 (Dimitrov et al. 2014), V342 Andromedae (Dimitrov et al. 2015) and DY Lyncis (Sekalska et al. 2010). For all these systems, we detected new spectroscopic components and modelled the eclipsing pairs. Here, we present the new results obtained for DY Lyn where we detected reflex motion due to the third body in the radial velocities (RVs) of the EB.

DY Lyncis (HD 65498) is a spectroscopic triple system containing an EB. The eclipses were originally detected by Maciejewski et al. (2003). They collected 232 photometric *V*-band measurements with the Semi-Automated Variability Search[1] (SAVS) instrument and obtained spectra with the 0.9-m Schmidt–Cassegrain telescope and Richardson slit spectrograph at Toruń Centre for Astronomy (Poland). The spectral range was 3800–5500 Å with a dispersion of 2 Å pix^{-1}, the pixel size of the 1024 × 256 CCD camera is 26 μm. They found that DY Lyn has an EA-type light curve, with a $1\overset{\circ}{.}3$ period and eclipses with similar depths of 0.4 mag. From the spectrum they estimated the spectral type to be F V.

The star is listed in the Tycho catalogue with colour index of the system $B - V = 0.47 \pm 0.05$ and the visual magnitude $9\overset{m}{.}78 \pm 0\overset{m}{.}04$. Photometric observations were also carried out by the All Sky Automatic Survey[2] (ASAS) and the Super WASP[3] project (Pollacco et al. 2006; Butters et al. 2010). Both light curves are of good quality and contain sufficient number of measurements for light-curve synthesis. The times of minima were measured by several authors.

⋆ E-mail: dimitrov@amu.edu.pl (WD); lehm@tls-tautenburg.de (HL); chrisk@amu.edu.pl (KK)

[1] http://www.home.umk.pl/~gmac/SAVS
[2] http://www.astrouw.edu.pl/asas
[3] http://wasp-planets.net

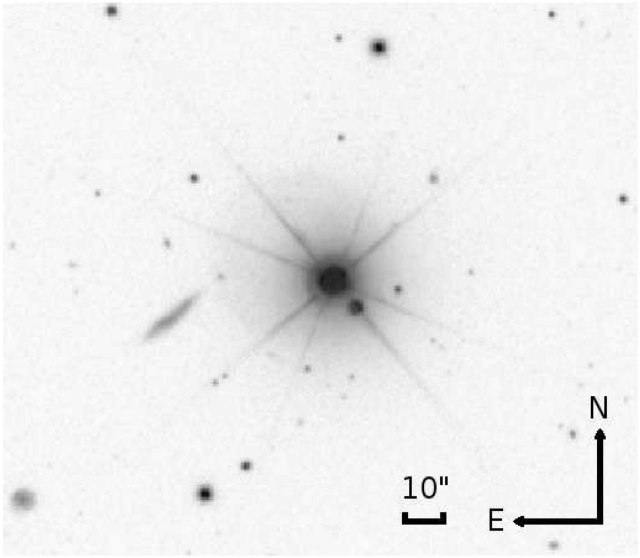

Figure 1. DY Lyn and its close visual companion (SDSS).

In a previous paper, Sekalska et al. (2010) showed that DY Lyn is a triple-lined star. This result was based on 13 echelle spectra obtained in 2009 with the 0.5-m Poznań Spectroscopic Telescope 1 (PST1; described in Baranowski et al. 2009). The authors determined the orbit of the EB and detected RV variations due to the third component. Based on the light curve and RV measurements, a preliminary Wilson–Devinney (WD) model was obtained. It shows two similar components with masses 1.02 and 1.05 $M_{\odot}$. As we know now, these results were influenced by the orbital motion of the three components around their common centre of mass (COM).

The main aim of our present research is, to confirm and measure the mutual orbital motions of the EB and the third component, to determine their orbits and the masses of the components, and to determine the atmospheric parameters and the chemical abundances of the components. Additionally, we want to investigate the close visual companion that is not mentioned in the visual binaries catalogues. This star, separated by about 9 arcsec from the spectroscopic triple (Fig. 1), might be a potential part of the DY Lyncis multiple system.

2 RADIAL VELOCITIES

2.1 Observations

We monitored the motion of the three components of DY Lyn over a period of six years. The first two spectroscopic data sets were collected with the 0.5-m PST1 and the 0.7-m PST2[4]. Both telescopes are equipped with fibre-fed echelle spectrographs having a resolving power of 40 000. The typical signal-to-noise ratio of the spectra is about 20, slightly better in the case of PST2. The spectral range for PST1 is 4325–7730 Å and 3880–9180 Å for PST2. Additionally, we obtained spectra with the coudé–echelle spectrograph at the 2-m telescope of the Thüringer Landessternwarte (TLS) Tautenburg, the data are described in Section 4.

The aims of the three telescopes were different. PST1 was used for long-term monitoring of the star. The second telescope's task was to acquire dense phase coverage of the short-period orbit. These data were also very useful for the determination of the period of the wide

[4] http://www.astro.amu.edu.pl/GATS

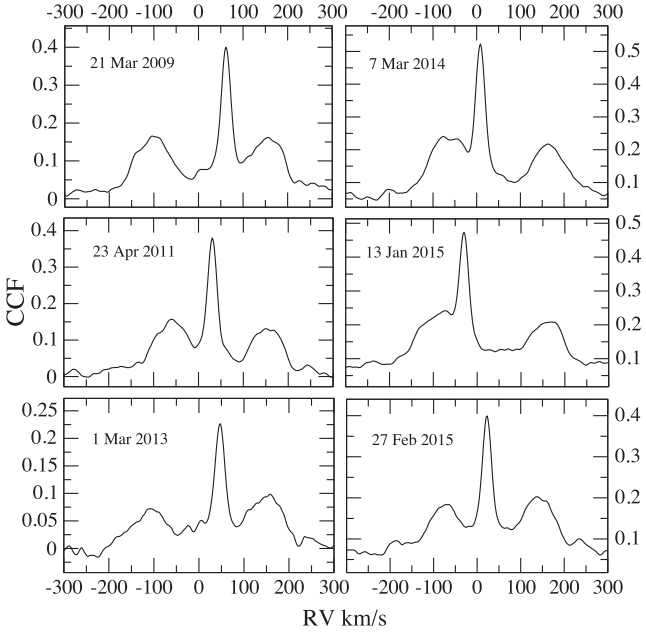

Figure 2. Cross-correlation functions for DY Lyncis obtained from the PST1/2 spectra showing the varying contributions from the three stars.

orbit. The third telescope (TLS), the biggest one, was used to obtain spectra with high signal-to-noise ratio (>400 for the decomposed spectra) and resolution (30 000) necessary for modelling the stellar atmospheres.

Data reduction for PST2 was made with the K. Kamiński code dedicated to this instrument. For PST1 we used IRAF/PYTHON scripts, and for cosmic ray removal the DCR code (Pych 2004). The RV measurements for all data sets were performed with the IRAF[5] FXCOR task that is based on the cross-correlation technique (Fig. 2). The velocities were measured by fitting three Gaussian functions to Cross Correlation Function (CCF) peaks. In some cases, the CCF was noisy and asymmetric. Additionally, we have blending of the three peaks in some phases. This reduces the precision and accuracy of RV measurements. The TLS spectra, which have better signal-to-noise ratio, were measured using both the FXCOR and the KOREL (Hadrava 1995) programs.

As we can see from Fig. 3, the measurements are influenced by the reflex motion. The RVs (FXCOR and KOREL results) are available at the CDS data base (cdsarc.u-strasbg.fr; Ochsenbein, Bauer & Marcout 2000).

2.2 Orbital solutions

The correction of the EB measurements for reflex motion due to the third component in its wide orbit was done iteratively. In the first step, we calculated the momentary velocity of the EB centre of mass (EB-COM) for every pair (V_1, V_2) of RVs of the EB components, starting with the mass ratio $q_{\rm EB} = 1$. We used the PHOEBE program (Prša & Zwitter 2005) based on the WD code (Wilson & Devinney 1971) to fit the wide orbit. From the synthetic curve of the EB-COM, we obtained the first corrections for our EB measurements. After the correction of the EB RV curves, we fitted the WD model for the close orbit and obtained a new value of the mass ratio

[5] IRAF is distributed by the National Optical Astronomy Observatory, which is operated by the Association of Universities for Research in Astronomy, Inc., under a cooperative agreement with the National Science Foundation.

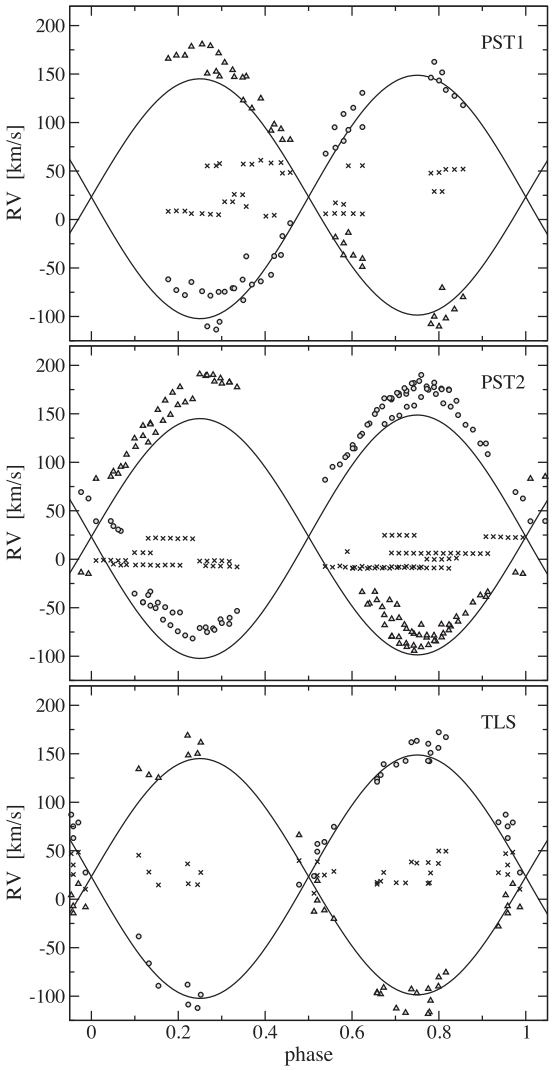

Figure 3. RV measurements before correcting for the 281-d wide orbit. Phased data from PST1 (top), PST2 (middle) and TLS (bottom). Solid lines represent the preliminary model by Sekalska et al. (2010) based on the first data set acquired in 2009. RVs obtained for EB_1, EB_2 and the third component are marked by circles, triangles and x signs, respectively.

that we used for the next iteration. During the process some outliers were rejected. After a few cycles we obtained the final, corrected RV curves (Figs 9 and 10).

We measured significant changes in the velocity of the third component, as well as in the systemic γ-velocity of the EB. We found that the third component is in an eccentric, long-period orbit with a period of 281 d. The semimajor axis is more than 44 times the one of the inner orbit. The results for the long-period orbit are listed in Table 1, while the orbital curves are shown in Fig. 4. The scatter of the EB-COM curve is considerable and significantly higher than the one of the third component. The eclipsing pair CCF peaks are broad and in many cases asymmetric, which causes this higher scatter. We searched for additional components in the residuals of both curves of the wide orbit, but without success.

In our first paper, as well as in the following work, we named the star with deeper photometric minimum (higher temperature) as component 1. A preliminary fit by Sekalska et al. (2010) yielded a mass ratio of 1.03 for the eclipsing pair. From the new results, corrected for the motion of EB-COM, we obtain $q_{EB} = m_2/m_1 = 0.94$.

Table 1. Parameters of the wide orbit derived with PHOEBE. The given errors are formal errors.

Parameter	Value
P (d)	281.18 ± 0.02
HJD_0	2454984.518 ± 0.148
$q = K_3/K_{EB}$	1.681 ± 0.027
$a \sin i\,(R_\odot)$	295.0 ± 1.8
$a \sin i$ (au)	1.372 ± 0.008
V_γ (km s^{-1})	31.76 ± 0.05
ω (rad)	4.213 ± 0.005
e	0.333 ± 0.001
K_3 (km s^{-1})	35.29 ± 0.04
K_{EB} (km s^{-1})	21.0 ± 0.4
$m_3 \sin^3 i\,(M_\odot)$	1.63 ± 0.03
$m_{EB} \sin^3 i\,(M_\odot)$	2.74 ± 0.04

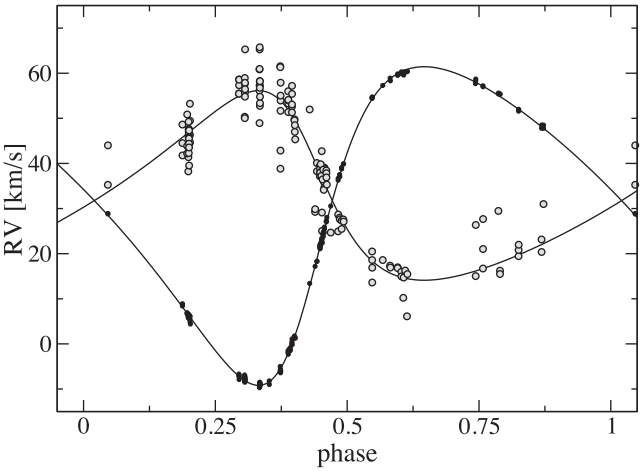

Figure 4. RVs of the EB-COM (open circles) and of the third component (black dots) phased with the 281-d period of the wide orbit.

Table 2. Available RVs and light curves. The σ_{RV} (rms of the eclipsing pair) for the TLS observations is given for both the RVs obtained from cross-correlation and with KOREL.

Instrument or project	HJD_{start} −2450000	HJD_{end} −2450000	Time span (d)	n_{obs}	$\sigma_{RV}/\sigma_{phot}$ (km s^{-1}/ mag)
Spectroscopy					
PST1	4912	6728	1816	37	3.7
PST2	6726	7106	380	82	3.2
TLS	7065	7125	60	34	3.0/0.6
Photometry					
SAVS	2695	2732	37	232	0.036
ASAS	3990	6915	2925	396	0.031
SWASP	3261	4575	1314	6230	0.018

3 LIGHT CURVES

Visual and broad-band light curves from three instruments are available for DY Lyncis. All instruments have a short focal length. Thus, the 15-mag visual companion separated by only 9 arcsec can contaminate the photometric measurements (Section 5.4). The data sets were collected by SAVS, ASAS and SWASP (Table 2). The last one

Table 3. Times of minima from literature.

HJD −2450000	Error	Cycle	O − C (d)	Source
2704.4884	0.0005	0	− 0.0006	Maciejewski et al. (2003)
3446.4341	0.0002	565	0.0025	Gurol et al. (2007)
3448.4039	0.0002	566.5	0.0025	Gurol et al. (2007)
4084.6343	0.0003	1051	0.0008	SWASP
4163.4226	0.0001	1111	− 0.0013	SWASP
4501.5646	0.0002	1368.5	− 0.0013	SWASP
4509.4451	0.0002	1374.5	0.0002	Brát et al. (2008)
4536.3681	0.0002	1395	0.0031	SWASP
4555.4088	0.0002	1409.5	0.0028	Brát et al. (2008)
4557.3791	0.0002	1411	0.0034	Brát et al. (2008)
4889.609	0.002	1664	0.001	Diethelm (2009)
4928.3437	0.0003	1693.5	− 0.0033	Brat et al. (2009)
5591.4958	0.0030	2198.5	− 0.0035	Hubscher (2011)
5640.7432	0.0004	2236	− 0.0000	Diethelm (2011)
6008.4321	0.0033	2516	0.0005	Hubscher, Braune & Lehmann (2013)
6012.3720	0.0025	2519	0.0009	Hubscher et al. (2013)
6282.8914	0.0016	2725	0.0067	Diethelm (2013)
6288.1368	–	2729	− 0.0006	Nagai (2013)
6322.2783	–	2755	− 0.0016	Nagai (2014)
6354.4512	0.0016	2779.5	− 0.0014	Hubscher (2013)
6356.4205	0.0005	2781	− 0.0019	Hubscher (2013)
6371.5211	0.0030	2792.5	− 0.0028	Hubscher (2013)
6698.5009	0.0021	3041.5	− 0.0030	Hubscher (2014)
6714.2589	0.0004	3053.5	− 0.0031	Hubscher & Lehmann (2015)
6746.4332	0.0018	3078	− 0.0015	Hubscher & Lehmann (2015)
7090.4888	0.0035	3340	0.0028	Hubscher (2016)

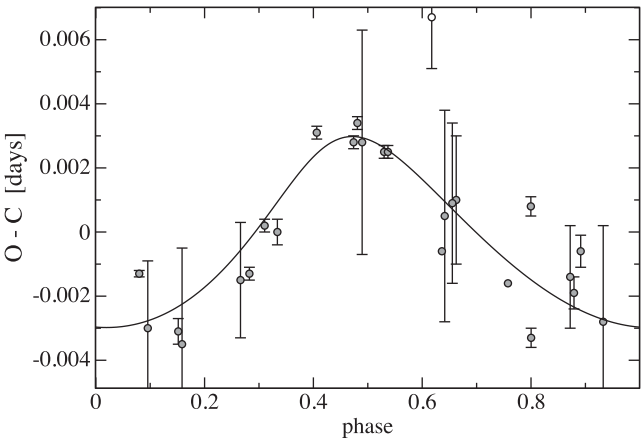

Figure 5. Times of minima phased with the orbital period of the wide orbit (281 d). The solid line represents a model calculated from the RV curve of the EB-COM.

has the best coverage and the lowest scatter, and we use it for modelling the system (Section 5). The SWASP data were collected with a broad-band filter with transmission range from about 400 to 700 nm, the centre of the band is near 550 nm (Pollacco et al. 2006).

Additionally, a few photometric measurements of times of minima exist in the literature (Table 3). The latest results published in 2015–2016, as well as the recently calculated SWASP minima, were not taken into account in the following ephemeris. The O − C diagram shows the light-time effect caused by the mutual orbital motion (Fig. 5). The peak-to-peak amplitude of the effect is about

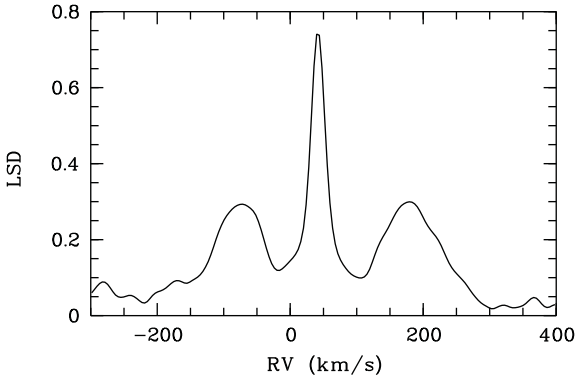

Figure 6. LSD profile computed from the TLS spectrum showing large separation of the components.

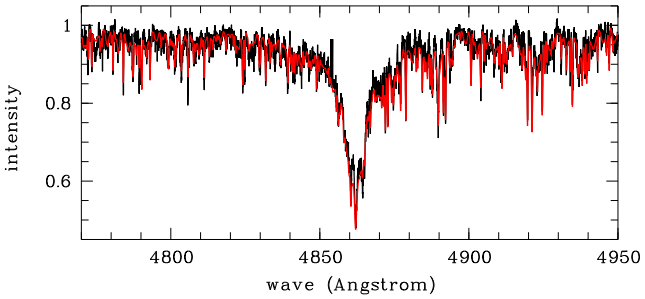

Figure 7. Best fit (red) of the Hβ region of DY Lyn (black) obtained from the spectrum analysis of one single spectrum.

500 s, which corresponds to a separation of about 1 au. There is good agreement between the observed photometric times of minimum and the synthetic curve calculated from the long-period spectroscopic orbit. The ephemeris calculated from the O − C residuals is

$$\min \mathrm{I} = \mathrm{HJD}\ 2452704.4890 + 1.31317274E. \quad (1)$$

4 SPECTRUM ANALYSIS

In a first step, we used the TLS spectrum showing the largest separation of the lines of the three components. Fig. 6 shows the least-squares deconvolution (LSD) profile computed from this spectrum. The profiles of the three components are clearly separated. We analysed this spectrum as described below. Fig. 7 shows the best fit obtained for the Hβ region.

In the next step, we used the KOREL program (Hadrava 1995) to disentangle the composite spectrum of DY Lyn based on the 34 spectra taken at TLS. Besides the decomposed spectra of the three components, KOREL also delivered the corresponding RVs. The decomposed spectra are normalized to the common continuum of the entire system and the local continua showed low-amplitude undulations as typical for Fourier-based programmes for spectral disentangling such as KOREL. The continua of the individual spectra were corrected for these undulations using spline functions. For the renormalization of the decomposed spectra, we need the continuum flux ratios between the components. These were computed during spectrum analysis together with the atmospheric parameters.

We analysed the decomposed spectra of the three components using the GSSP program (see Lehmann et al. 2011 and Tkachenko et al. 2012 for a description of the method). The program is based

Table 4. Results of spectrum analysis for the third and the two EB components. f is the flux ratio compared to the total continuum flux. The values in the lower part are derived for fixed $[M/\mathrm{H}] = 0$ and equal $\log g$ of the EB components.

		C3	EB1	EB2
$[M/\mathrm{H}]$	(dex)	-0.02 ± 0.10	0.02 ± 0.15	-0.11 ± 0.16
$T_{\rm eff}$	(K)	6390 ± 140	6427 ± 180	6173 ± 230
$\log g$	(cgs)	4.07 ± 0.35	4.42 ± 0.42	4.09 ± 0.46
$v_{\rm turb}$	(km s^{-1})	1.28 ± 0.34	1.64 ± 0.83	1.1 ± 1.0
$v \sin(i)$	(km s^{-1})	12.8 ± 1.4	60.3 ± 6.0	58.3 ± 7.0
f		0.422	0.306	0.272
$T_{\rm eff}$	(K)	6380 ± 110	6370 ± 150	6260 ± 140
$\log g$	(cgs)	4.10 ± 0.31	4.2 fixed	4.2 fixed
$v_{\rm turb}$	(km s^{-1})	1.24 ± 0.34	1.43 ± 0.69	0.93 ± 0.90
$v \sin i$	(km s^{-1})	12.8 ± 1.4	60.2 ± 6.0	58.2 ± 7.0
f		0.429	0.306	0.265

on the spectrum synthesis method. We extended the method to a simultaneous fit of three components in a composite spectrum or three decomposed spectra of the components. The synthetic spectra were computed on the TLS cluster computer with the parallelized version of the SYNTHV program (Tsymbal 1996), based on LLmodels atmospheres (Shulyak et al. 2004). The atomic data were taken from the VALD data base (Kupka et al. 1999). We used three grids of atmospheric parameters, one for each component. Free parameters were $[M/\mathrm{H}]$, $T_{\rm eff}$, $\log g$, $v_{\rm turb}$ and $v \sin i$. These parameters were optimized by searching for the minimum in χ^2. The optimum continuum flux ratios between the components were determined for each grid point from least-squares minimization.

We used scaled solar abundances for the surface metallicities $[M/\mathrm{H}]$. After getting the best solution, we added the individual abundances of single chemical elements to our grid of free parameters, optimizing the abundances element by element and repeating this process until the changes in χ^2 became negligible. After the final optimum solution in all free parameters was found, the parameter errors were determined from χ^2 statistics using the full grid of atmospheric parameters plus [Fe/H] in the vicinity of the optimum solution. In this way, the errors include all interdependences between the parameters. We had not the computer power to also count for the interdependences between the parameters of different components, however, which are coupled via the flux ratios.

Table 4 lists the results, obtained from the 455–567 nm spectral region. There are two reasons why we prefer this solution against the results obtained from the analysis of the single, composite spectrum. First, the parameter errors are smaller. And, more important, whereas the single-spectrum analysis ended up with different $[M/\mathrm{H}]$ of the components reaching from -0.4 to -0.1, the analysis of the decomposed spectra yields a consistent solution providing almost the same values for all three components. We assume that the single spectrum did not allow us to include the optimization of the surface abundances into the analysis. The number of free parameters was simply too large and the strong interdependence between $[M/\mathrm{H}]$ (mainly [Fe/H]) and $T_{\rm eff}$ prevented us from finding a reliable solution.

$[M/\mathrm{H}]$, $T_{\rm eff}$, $\log g$and $v_{\rm turb}$ of all three components agree within 1σ. The masses and radii of EB1 and EB2 are about the same, but the difference in $\log g$ disagrees with the calculated flux ratio. Assuming the same $\log g$ for both components, we get, from the Stefan–Boltzmann law, a flux ratio of approximately $(T_{\rm EB2}/T_{\rm EB1})^4 = 0.88$, in agreement with the computed flux ratio of 0.89. Here, we can neglect the different bolometric corrections for the two stars

Table 5. Abundances for DY Lyn components. Elemental abundances used for the Sun and abundances relative to these values in dex for the third component and the two EB components.

El.	Sun	C3	EB1	EB2
Fe	-4.59	$-0.02^{+0.09}_{-0.10}$	$0.00^{+0.12}_{-0.13}$	$-0.11^{+0.13}_{-0.14}$
Cr	-6.40	$+0.08^{+0.20}_{-0.23}$	$+0.01^{+0.29}_{-0.37}$	$-0.14^{+0.32}_{-0.40}$
Ni	-5.81	$-0.03^{+0.20}_{-0.23}$	$+0.02^{+0.31}_{-0.39}$	$-0.04^{+0.32}_{-0.42}$
Mg	-4.51	$+0.08^{+0.23}_{-0.27}$	$+0.11^{+0.23}_{-0.29}$	$-0.23^{+0.26}_{-0.34}$
Ti	-7.14	$-0.03^{+0.23}_{-0.26}$	$-0.14^{+0.39}_{-0.43}$	$-0.15^{+0.39}_{-0.53}$
Ca	-5.73	$+0.04^{+0.40}_{-0.45}$	$+0.06^{+0.61}_{-0.79}$	$-0.09^{+0.63}_{-0.88}$
Mn	-6.65	$+0.10^{+0.43}_{-0.54}$	–	–

that are justified by the small difference in $T_{\rm eff}$ (from Torres 2010, we get $\triangle BC = 0.01$ mag for a difference of 100 K in this range of $T_{\rm eff}$). We therefore searched for the solution of lowest χ^2 by fixing $\log g$ of both EB1 and EB2 to 4.2 and setting $[M/\mathrm{H}] = 0$ for all three components. The results are listed in the lower part of Table 4.

Table 5 lists the derived abundances. They all, as well as the derived surface metallicities, agree with the solar ones within the measurement errors. Solar values are based on Asplund, Grevesse & Sauval (2005). The SYNTHV program uses [A/N], i.e. the logarithm of numbers of atoms of an element compared to the total number of all atoms (one has to add 12.04 to get the Asplund et al. 2005 values).

A simple check of the flux ratios comparing the values obtained from spectrum analysis with the theoretical values as they follow from the atmospheric parameters can be obtained using

$$f_i \sim M_i \, T_i^4 \, 10^{-\log(g_i)} \qquad (2)$$

together with $\sum(f_i) = 1$ and neglecting the bolometric corrections as before. If we take the masses of the components from Tables 1 and 6 and the other parameters from the lower part of Table 4, we get $f_{\rm EB1} = 0.30, f_{\rm EB2} = 0.26$ and $f_{\rm comp3} = 0.44$. This is in good agreement with the flux ratios that we derived from spectrum analysis.

5 MODELLING OF THE SYSTEM

5.1 The eclipsing pair

The new spectroscopy enabled us to revise our preliminary model of the system (Sekalska et al. 2010). We know now that the third body is orbiting the EB pair in a wide, 281-d orbit and that the peak-to-peak velocity amplitude measured from the COM is 56 km s^{-1}. That means the data cannot be analysed without correcting for this motion. For the modelling, we again used the PHOEBE program. We assumed a circular orbit and synchronous rotation, based on the short period and tidal interaction of the components that cause fast circularization and synchronization. We applied parameters for gravity brightening and reflection consistent with a convective envelope (the spectral type is about F7.5) using $g_{12} = 0.32$, $a_{12} = 0.5$. For the calculation of the limb darkening effect, we used the logarithmic law and van Hamme (1993) coefficients. The SWASP data were collected with a broad-band filter centred at 550 nm. We used visual-band limb darkening coefficients, which is an approximation. We checked that this yields an error in radii less than 0.5 per cent. We included 6230 SWASP photometric measurements into the calculations (Fig. 8). This is the best available light curve with $\sigma_{\rm LC} = 0.018$ mag. We used 286 RV measurements (both components), corrected for the motion around the COM of the whole system (Fig. 9).

Table 6. Results of the modelling of DY Lyncis with the WD method and derived absolute parameters. Third light (l_3) corresponds to additional contributions; mainly from the third star, plus light from the visual companion (Section 5.4). For the WD results, additionally, the bootstrap errors are given.

Parameter	Eclipsing pair		Bootstrap
	Comp. 1	Comp. 2	error
WD results			
Period	$1\overset{d}{.}313\,1727(4)$		
i_{EB}	$88\overset{\circ}{.}95 \pm 0.18$		± 0.10
q_{EB}	0.940 ± 0.001		± 0.005
a_{EB} ($R_\odot$)	6.704 ± 0.004		± 0.012
Ω	6.374 ± 0.023	5.734 ± 0.017	$\pm 0.019/\pm 0.020$
$l_{1,2}$	0.3063 ± 0.0016	0.3056 ± 0.0016	$\pm 0.0014/\pm 0.0013$
l_3	0.3882 ± 0.0016		± 0.0009
Absolute parameters			
Mass ($M_\odot$)	1.212 ± 0.003	1.140 ± 0.002	$\pm 0.010/\pm 0.009$
Radii ($R_\odot$)	1.240 ± 0.006	1.350 ± 0.003	$\pm 0.010/\pm 0.010$
T_{eff} (K)	6370 fixed	6120 ± 150	
M_{bol}	3.90 ± 0.11	3.89 ± 0.11	
log g (cgs)	4.340 ± 0.005	4.240 ± 0.002	$\pm 0.011/\pm 0.010$

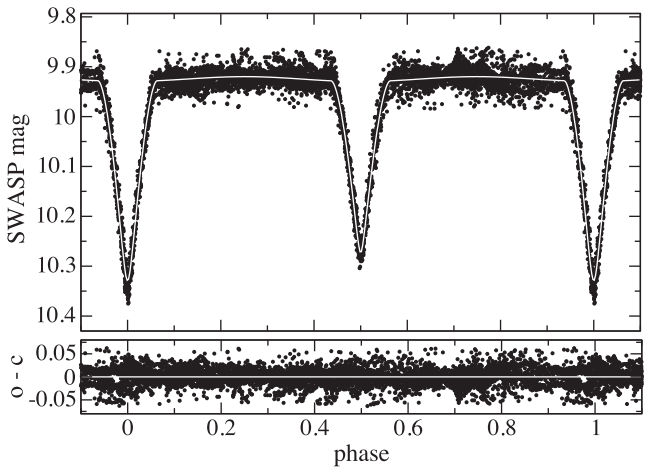

Figure 8. SWASP photometric data and the fitted light curve.

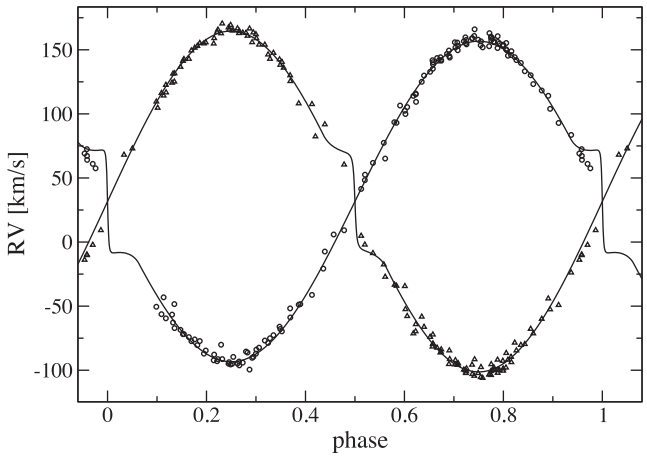

Figure 9. RVs from all three telescopes obtained from cross-correlation and the fitted orbital curve of the EB.

The dispersion of these measurements is $\sigma_{RV} = 3.29$ km s^{-1}. Some of the RVs near phase 0.95 are discrepant. This could be caused by the strong blending of CCF peaks close to the eclipse phases.

Our best fit yields two very similar stars with masses of 1.21 and 1.14 $M_\odot$. The components are only slightly distorted, the curvature of the light curve in out-of-eclipse phases is very small. The obtained model differs significantly from the results published in Sekalska et al. (2010) because, as already mentioned, the authors did not take the mutual orbital motion into account. For calculation of the bootstrap errors, we used a random reselection of the measurements. This way we obtained ten $RV_{1,2}$ and LC curves. We fit the model for every new data set and calculated 1σ errors from the scatter of the results. The relatively small noise in the LC and RV data gave us errors for the absolute parameters of about 1 per cent or less. But we must keep in mind that the accuracy could be worse. The discrepancy of the results for both orbits, probably caused by blending of lines, shows that we have some systematic problems.

The total mass of the EB of 2.35 $M_\odot$ disagrees with the lower mass limit of 2.74 $M_\odot$ obtained from the wide-orbit solution. Another question that arises is that about the too large radius of the secondary component, which was confirmed by tests with other photometric data sets. Both problems will be discussed in Sections 5.2 and 5.3.

We additionally applied the KOREL program to the spectra with best signal-to-noise ratio (TLS). The results are compared with those from cross-correlation in Table 7. Obtained mass ratios and semimajor axes differ by about 1 per cent. The fitted curves are shown in Fig. 10. The apparent difference in the γ-velocities comes from the fact that KOREL delivers the RVs on a relative scale only.

We searched for additional short-term variability in the SWASP data. We subtracted the WD model for the EB variability from the data. For the period analysis, we used a code written by Gracjan Maciejewski that is based on the Schwarzenberg-Czerny (1996) method. We did not find any significant periodic brightness changes of the system.

5.2 The third component

We use the term 'third component' for the companion of the EB pair. This star is the most luminous component in the system. Most of

Table 7. Results from fitting the EB spectroscopic data from all telescopes using cross-correlation and from the TLS data using KOREL.

Parameter	All instruments cross-correlation	TLS KOREL
q_{EB}	0.940 ± 0.001	0.950 ± 0.002
a_{EB} ($R_\odot$)	6.704 ± 0.004	6.661 ± 0.008
V_γ (km s^{-1})	31.69 ± 0.06	0.002 ± 0.136
Period (d)	1.313 1732(4)	1.313 145(27)
HJD_0	2457065.5366(2)	2457065.5368(6)
K_1 (km s^{-1})	125.1 ± 0.1	125.0 ± 0.3
K_2 (km s^{-1})	133.1 ± 0.1	131.6 ± 0.3
σ_{rv} (km s^{-1})	3.3	0.6

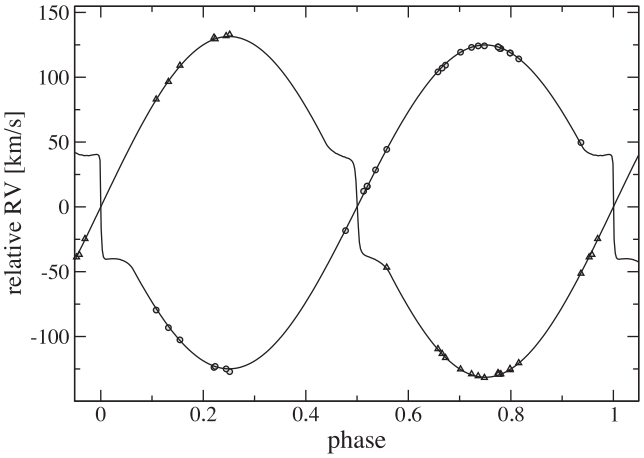

Figure 10. TLS RVs obtained with KOREL and the fitted orbital curve of the EB.

Table 8. Mass estimation for the third component.

Method/Based on	m_3 value
Wide-orbit m_3 lower limit	>1.63 ± 0.03 $M_\odot$
Wide-orbit mass ratio and close orbit EB mass	1.40 ± 0.02 $M_\odot$
Spectrum analysis	1.44 ± 0.05 $M_\odot$

the information that we have for it comes from the spectral analysis (Section 4). We obtained T_{eff} = 6380±110 K, log g = 4.10±0.31, $v \sin i$ = 12.8±1.4 km s^{-1} and the continuum flux ratio of f = 0.429 (Table 4).

Additionally, we derived the information about its mass from the long-period orbit. The value of the product $m_3 \sin^3 i$ is 1.63 ± 0.03 $M_\odot$ (Table 1). So the lower limit for the mass is 1.63 $M_\odot$. We must be careful with the mass of the third component, because we observe a discrepancy between the masses coming from the close and wide orbits. Therefore, we made some additional estimations of the third body mass (compared in Table 8). The first one, in our opinion the most reliable, is based on the wide-orbit mass ratio and the mass of the EB from the close orbit, giving 1.40 $M_\odot$.

The second estimation is based on the evolutionary tracks and results of the spectrum analysis. We found that the mass of the third component must be 1.44 $M_\odot$ to be in agreement with the log g and log(T) values from the spectrum analysis. Additionally, we have the estimation of the continuum flux ratio f_3 = 0.429 (Table 4) and the so-called third light from the WD model l_3 = 0.388 (Table 6). If the mass of the third body is 1.63 $M_\odot$, its luminosity will be almost

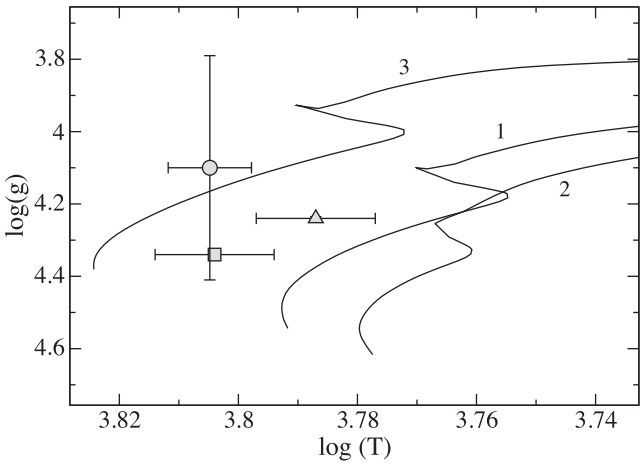

Figure 11. Evolutionary Yonsei–Yale tracks for all three components of the DY Lyncis system, calculated for masses 1.40, 1.212 and 1.140 $M_\odot$ and metallicity z = 0.23. The square and triangle refer to the primary and secondary EB components, respectively, while the circle represents the third body. The log g error bars for the EB components are smaller than their symbols.

three times higher than the one of the main EB component. The f_3 and l_3 estimations show that the luminosity of the third component must be lower than this, i.e. the star must have a lower mass. Based on these additional considerations, we estimate the mass of the third component to 1.40 $M_\odot$.

Looking for an explanation of the fact that the mass calculated from the wide orbit is significantly higher than the one calculated from the inner orbit, we searched for alternative periods of both orbits, but without success. The results were additionally checked and confirmed by using other codes such as KOREL and FOTEL. We also checked our procedure for correction of the EB RVs for the reflex motion due to the third component. We tested the possibility whether an incorrect value of the inclination of the small orbit is responsible for the mass discrepancy. The disagreement disappears for $i \sim 75^\circ$; however, for such inclination it is impossible to find a proper photometric solution. Alternatively, we can search for an explanation in the data accuracy. As we mentioned earlier, the EB-COM curve has a considerable scatter. The obtained mass of the EB is sensitive to the K_{EB} value. If the amplitude K_{EB} is only 3.5 km s^{-1} lower, the discrepancy between the results calculated from the two orbits disappears. We also considered the possibility that one more component might exist in the system. Such a scenario, however, is less likely.

Using the mass and log g, we estimate the stellar radius $R_3 = 1.7^{+0.7}_{-0.5}$ $R_\odot$. The value of log g and the corresponding radii are in good agreement with the evolutionary track (Fig. 11). From the spectroscopy, we know that the third star is orbiting the COM of the system in an eccentric orbit (e = 0.33) with a period of 281 d.

5.3 Distance and age of the system

No parallaxes are given for this system in the *Hipparcos* catalogue, as well as in the literature. We used the photometric parallax to estimate the distance. For brightness determination of the three components, we took the values (radii and temperatures) from our WD model (Table 6), as well as the values from the spectrum analysis for the third component (Table 4). We obtained a parallax of 3.5 ± 0.7 mas, corresponding to 285 ± 66 pc. The recently realized Tycho-Gaia Astrometric Solution (Gaia Collaboration et al. 2016;

Table 9. Stars in 30 arcsec radius around DY Lyncis coordinates, according to GSC 2.3.2 catalogue. The first line corresponds to DY Lyn and the next three lines to the visual companions. The first column presents the angular separation from DY Lyn.

Separation (arcsec)	RA (^{hms})	DEC ($^{\circ\prime\prime}$)	*F* mag Red	*Bj* mag Blue	*V* mag Visual	*N* mag 0.8 μm
–	08 00 45.954	+42 10 33.05	–	–	9.82	–
2.4	08 00 46.132	+42 10 31.68	–	–	–	10.93
9.3	08 00 45.395	+42 10 26.16	–	15.28	14.57	13.32
20.7	08 00 44.105	+42 10 31.14	17.49	19.15	–	17.00

Lindegren et al. 2016) catalogue provides a new parallax value for DY Lyn of 4.14 ± 0.29, which corresponds to the distance of 242 ± 16 pc. These values are in agreement, within errors, with our result.

We calculated the evolutionary tracks for the three components using the Yonsei–Yale[6] results (Yi et al. 2001; Kim et al. 2002; Yi, Kim & Demarque 2003). We applied masses from the WD model for the EB components and used mass estimation based on the mass ratio of the wide orbit (Table 8) for the third component. Basing on the spectrum analysis (Section 4), we applied solar metallicities for all three components. Fig. 11 shows their tracks together with the positions of the stars. The positions of the EB components are based on the WD results (Table 6) and that of the third component on spectrum analysis (Table 4, lower part). The most massive component is close to its track and we estimate its age as ∼2.5 Gyr, which is probably the age of the whole system. The plot suggests that all three stars are in the core hydrogen burning stage, i.e. still on the main sequence. The third component lies close to its track, while the EB components are shifted to higher temperatures. This suggests that masses of the EB components could be underestimated. The shift could be connected with the discrepancy between the results of the wide and close orbits. The big difference between the $\log g$ error bars for the three stars comes from the different methods used for calculation of the parameter. The radii of the secondary component of the EB derived from both WD and spectrum analysis (upper part of Table 4) are higher than we expected.

5.4 Potential visual companions

As we mentioned in the introduction, DY Lyncis has a close visual companion separated by about 9 arcsec. The star is listed in the Guide Star Catalogue (GSC; Lasker et al. 2008) as N8UM017674, with a brightness of 15 mag. A rough estimation of the distance between the components, assuming that they are gravitationally bound, gives a separation of $\sim 2.7 \times 10^3$ au. We can estimate the distance to the visual companion using the photometric parallax method. We used the colour index $B - V = 0.71$ (photometric measurements are listed in Table 9). Assuming that the star is on the main sequence, we found that its spectral type is G 6.5 and the photometric parallax gives a distance of more than 700 pc. This means that the star cannot belong to the DY Lyncis system.

A search in the GSC in the neighbourhood of DY Lyn (Table 9) allows us to find a very close and relatively bright visual companion in only 2.4 arcsec distance. Assuming that this star is a part of the system, we can estimate that this distance corresponds to ∼680 au. Thus, this companion cannot be the third component of DY Lyncis, which is brighter and has a distance from the EB of about 300 $R_\odot$ (∼1.4 au). The star is fainter than the limiting magnitude of the PST1/2 telescopes used for spectroscopy and was also not detected in the spectra obtained with the bigger TLS telescope. It could be a field star, as well as part of the DY Lyncis system. Since we have no information about its luminosity, the answer is left for future investigation.

[6] http://www.astro.yale.edu/demarque/yystar.html

6 SUMMARY AND CONCLUSIONS

DY Lyncis is a hierarchical triple system. The preliminary results based on the WD method that were published in Sekalska et al. (2010) were affected by the motion of the third component. We performed the first long-term spectroscopic observational campaign of this system. Correcting the RVs for the reflex motion around the COM of the system, we now derived revised solution for the close orbit of the EB and the first solution for the wide orbit of the third component. From spectrum analysis, we obtained the temperatures and metallicities of all three components. Applying the WD model, the masses and radii of the EB were determined with a precision of about 1 per cent, but the accuracy could be worse because of the systematic error in RV measurements. The short-period ($1^d.3$) orbit is circular, while the 281-d orbit of the third component is eccentric with $e = 0.3$.

The results of our analysis raise two questions that are still open. The first is about the discrepancy between the mass of the EB calculated from the WD model for the close orbit and the minimal EB mass following from the wide orbit. Careful analysis of possible alternative orbital periods and tests of obtained amplitudes and inclination confirm the obtained results. The most probable explanation of the discrepancy is a systematic error in RV measurements caused by blending broad and asymmetric EB peaks in a cross-correlation function.

The second point is the larger radius of the lower mass EB component, which follows from our analysis, as well as from an additional analysis of other available curves (ASAS, SAVS). Despite many tests, we did not find the final answers for these two questions and we leave it for the future analysis.

ACKNOWLEDGEMENTS

We are grateful to our engineer Roman Baranowski and to Tomasz Kwiatkowski and Alexander Schwarzenberg-Czerny, the founders of the Poznań Spectroscopic Telescope project. We thank Waldemar Ogłoza for making the times of minima and the ephemeris of DY Lyn available for our studies. This work was supported by the Polish National Science Centre through grant UMO-2011/01/D/ST9/00427.

This work is based on spectroscopy obtained at the Poznań Spectroscopic Telescope 1 and 2, Poland, Thüringer Landessternwarte, Tautenburg, Germany and SWASP photometry.

This work has made use of data from the European Space Agency (ESA) mission *Gaia* (http://www.cosmos.esa.int/gaia),

processed by the *Gaia* Data Processing and Analysis Consortium (DPAC, http://www.cosmos.esa.int/web/gaia/dpac/consortium). Funding for the DPAC has been provided by national institutions, in particular the institutions participating in the *Gaia* Multilateral Agreement.

REFERENCES

Asplund M., Grevesse N., Sauval A. J., 2005, in Barnes T. G., III, Bash F. N., eds, ASP Conf. Ser. Vol. 336, Cosmic Abundances as Records of Stellar Evolution and Nucleosynthesis. Astron. Soc. Pac., San Francisco, p. 25
Baranowski R. et al., 2009, MNRAS, 396, 2194
Brát L. et al., 2008, Open Eur. J. Var. Stars, 94, 1
Brat L. et al., 2009, Open Eur. J. Var. Stars, 107, 1
Butters O. W. et al., 2010, A&A, 520, L10
Diethelm R., 2009, Inf. Bull. Var. Stars, 5894, 1
Diethelm R., 2011, Inf. Bull. Var. Stars, 5992, 1
Diethelm R., 2013, Inf. Bull. Var. Stars, 6042, 1
Dimitrov W. et al., 2014, A&A, 564, A26
Dimitrov W. et al., 2015, A&A, 575, A101
Eggleton P. P., Kiseleva-Eggleton L., 2001, ApJ, 562, 1012
Gaia Collaboration et al., 2016, A&A, 595, A2
Gurol B. et al., 2007, Inf. Bull. Var. Stars, 5791, 1
Hadrava P., 1995, A&AS, 114, 393
Hubscher J., 2011, Inf. Bull. Var. Stars, 5984, 1
Hubscher J., 2013, Inf. Bull. Var. Stars, 6084, 1
Hubscher J., 2014, Inf. Bull. Var. Stars, 6118, 1
Hubscher J., 2016, Inf. Bull. Var. Stars, 6157, 1
Hubscher J., Lehmann P. B., 2015, Inf. Bull. Var. Stars, 6149, 1
Hubscher J., Braune W., Lehmann P. B., 2013, Inf. Bull. Var. Stars, 6048, 1
Kim Y.-C., Demarque P., Yi S. K., Alexander D. R., 2002, ApJS, 143, 499
Kohler R., Leinert C., 1998, A&A, 331, 977
Kupka F., Piskunov N., Ryabchikova T. A., Stempels H. C., Weiss W. W., 1999, A&AS, 138, 119
Lasker B. M. et al., 2008, AJ, 136, 735
Lehmann H. et al., 2011, A&A, 526, A124
Leinert C., Zinnecker H., Weitzel N., Christou J., Ridgway S. T., Jameson R., Haas M., Lenzen R., 1993, A&A, 278, 129
Lindegren L. et al., 2016, A&A, 595, A5
Maciejewski G., Czart K., Niedzielski A., Karska A., 2003, Inf. Bull. Var. Stars, 5431, 1
Nagai K., 2013, Var. Star Bull., 55. Available at: http://vsolj.cetus-net.org/bulletin.html
Nagai K., 2014, Var. Star Bull., 56. Available at: http://vsolj.cetus-net.org/bulletin.html
Ochsenbein F., Bauer P., Marcout J., 2000, A&AS, 143, 23
Pollacco D. L. et al., 2006, PASP, 118, 1407
Prša A., Zwitter T., 2005, ApJ, 628, 426
Pych W., 2004, PASP, 116, 148
Schwarzenberg-Czerny A., 1996, ApJ, 460, L107
Sekalska J. et al., 2010, Inf. Bull. Var. Stars, 5954, 1
Shulyak D., Tsymbal V., Ryabchikova T., Stütz C., Weiss W. W., 2004, A&A, 428, 993
Tkachenko A., Lehmann H., Smalley B., Debosscher J., Aerts C., 2012, MNRAS, 422, 2960
Torres G., 2010, AJ, 140, 1158
Tsymbal V., 1996, in Adelman S. J., Kupka F., Weiss W. W., eds, ASP Conf. Ser. Vol. 108, M.A.S.S.; Model Atmospheres and Spectrum Synthesis. Astron. Soc. Pac., San Francisco, p. 198
van Hamme W., 1993, AJ, 106, 2096
Wilson R. E., Devinney E. J., 1971, ApJ, 166, 605
Yi S., Demarque P., Kim Y.-C., Lee Y.-W., Ree C. H., Lejeune T., Barnes S., 2001, ApJS, 136, 417
Yi S. K., Kim Y.-C., Demarque P., 2003, ApJS, 144, 259
Zasche P., Wolf M., Hartkopf W. I., Svoboda P., Uhlař R., Liakos A., Gazeas K., 2009, AJ, 138, 664

This paper has been typeset from a TEX/LATEX file prepared by the author.